A network of *cis* and *trans* interactions is required for ParB spreading

Dan Song, Kristen Rodrigues, Thomas G.W. Graham, and Joseph J. Loparo

Supplementary Information

- Supplementary Materials and Methods
- Supplementary Tables
- Supplementary Figure Legends
- Supplementary References
- Supplementary Figures

SUPPLEMENTARY MATERIALS AND METHODS

Immunoblot analysis

Vegetatively growing cells were harvested at OD_{600} between 0.3 and 0.4, and 1 ml of cells were collected and resuspended in lysis buffer (20 mM Tris at pH 7.5, 1 mM EDTA, 10 mM $MgCl_2$, 1 mg/ml lysozyme, 1 mM PMSF, 10 µg/ml DNase I and 100 µg/ml RNase A) to a final OD_{600} of 20 for equivalent loading. The cells were incubated at 37°C for 10 min followed by addition of equal volume of sodium dodecyl sulfate (SDS) sample buffer (0.25 M Tris at pH 6.8, 4% SDS, 20% glycerol, 10 mM EDTA and 1% bromophenol blue) containing 10% 2-mercaptoethanol. Samples were heated for 5 min at 80°C prior to loading. Proteins were separated by SDS-PAGE on 12% precast polyacrylamide gels (BioRad), electroblotted onto polyvinylidine fluoride membranes, and blocked in 5% nonfat milk in 1x phosphate-buffered saline-0.05% Tween-20 (PBST). The blocked membranes were probed with anti-GFP (1:10,000) (Rudner *et al.* 1999), anti-Spo0J (1:5,000) (Lin *et al.* 1997), or anti-SigA (1:10,000) (Fujita 2000) antibodies diluted into 3% BSA in PBST. Primary antibodies were detected using 1:20,000 horseradish peroxidase (HRP)-conjugated rabbit anti-mouse IgG (H + L) secondary antibody (Jackson ImmunoResearch) in 5% nonfat milk in PBST. Blots were exposed to chemiluminescent HRP substrate (HyGLO Quick Spray, Denville Scientific) and imaged on an Amersham Imager 600 (GE Healthcare Life Sciences). Blots with weak signal were re-imaged using SuperSignal West Femto Maximum Sensitivity Substrate (Thermo Scientific).

Size exclusion chromatography with multi-angle light scattering

Wild type *Bs*Spo0J proteins at 120 µg ml^{-1} and BSA standard at 2 mg ml^{-1} were run at a flow rate of 0.5 ml min^{-1} in storage buffer (20 mM Tris at pH 8.0, 350 mM NaCl, 10% glycerol, 10 mM imidazole and 5 mM BME) on an AdvanceBio 300Å size exclusion chromatography column (Agilent Technologies) attached to an Agilent 1260 Infinity Isocratic Liquid Chromatography System (Agilent Technologies) coupled with a Wyatt Dawn Heleos II Multi-Angle Light Scattering detector (Wyatt Technology) and a Wyatt Optilab T-rex Refractive Index Detector (Wyatt Technology). Chromatograms were analyzed using the ASTRA 7 software (Wyatt Technology) to determine the molecular weights.

Plasmid construction

Variants of **pKM304** (Graham *et al.* 2014) encoding mutants of His6-SUMO-*Bs*Spo0J were generated by site-directed mutagenesis (either QuickChange or Round-the-Horn method) with primers listed in Supplementary Table S4. Sequences of the resulting constructs were confirmed with universal T7-sequencing primers.

Variants of **pWX563** (Graham *et al.* 2014) encoding mutants of mGFPmut3-*Bs*Spo0J were generated by site-directed mutagenesis (either QuickChange or Round-the-Horn method) with primers listed in Supplementary Table S4. Sequences of the resulting constructs were confirmed with either primer oTG237 or primer oTG004R.

pLS063 was generated from **pLS050** by site-directed mutagenesis (QuickChange method) with primers oTG169 and oTG170.

pLS064 was generated from **pLS050** by site-directed mutagenesis (QuickChange method) with primers oLS077F and oLS077R.

pLS066 was generated from **pTG240** by site-directed mutagenesis (QuickChange method) with primers oTG169 and oTG170.

pLS067 was generated from **pTG240** by site-directed mutagenesis (QuickChange method) with primers oLS077F and oLS077R.

SUPPLEMENTARY TABLES

Supplementary Table S1: Mutations introduced in this study

Residue in *Hp*Spo0J	Residue in *Bs*Spo0J	Identity	Mutation(s) in *Bs*Spo0J	References
R49	R39	Interaction hub	R39A	This work
Q62	E52	Interacting partner	E52R	This work
H67	H57	Interacting partner	H57E	This work
L70	L60	Interaction hub	L60E	This work
Q71	Q61	Interaction hub	Q61A, Q61R	This work
P72	P62	Interaction hub	P62A	This work
Y82	Y72	ParB Box II	Y72A	This work
L84	I74	Interaction hub; ParB Box II	I74A	This work
I85	V75	Interaction hub; ParB Box II	V75A, V75E	This work
G87	G77	Interacting partner; ParB Box II	G77S	Breier and Grossman 2007; Graham *et al*. 2014
E88	E78	Interaction hub; ParB Box II	E78R	This work
R89	R79	Interaction hub; ParB Box II	R79A	Graham *et al*. 2014
R90	R80	Interaction hub; ParB Box II	R80A	Autret *et al.* 2001; Graham *et al*. 2014
L91	F81	Interaction hub; ParB Box II	F81A	This work
R92	R82	Interaction hub; ParB Box II	R82A	Graham *et al*. 2014
M114	M104	Interacting partner	M104A	This work
R115	R105	Interaction hub	R105A, R105E	This work
N122	N112	Interacting partner	N112S	Gruber and Errington 2009
E150	Q140	Interaction hub	Q140A, Q140R	This work

Supplementary Table S2: Strains used in this study

Strain	Genotype	Source	Figure
PY79	wild type	Youngman *et al.* 1983	S2
BDR2292	*Δspo0J::spec*	Wang *et al.* 2015	
BWX523	*sacA::hbsu-mcherry kan*	X.W. and D.Z.R., unpublished	
BDR2798	*pelB::Psoj-mgfpmut3-spo0J **WT** (ΔparS) tet, Δspo0J::spec, sacA::hbsu-mcherry kan*	Graham *et al.* 2014	2, S3 – S5, S20
BDR2796	*pelB::Psoj-mgfpmut3-spo0J **G77S** (ΔparS) tet, Δspo0J::spec, sacA::hbsu-mcherry kan*	Graham *et al.* 2014	2, S4
BDR2797	*pelB::Psoj-mgfpmut3-spo0J **R79A** (ΔparS) tet, Δspo0J::spec, sacA::hbsu-mcherry kan*	Graham *et al.* 2014	2, S3
BDR2799	*pelB::Psoj-mgfpmut3-spo0J **R80A** (ΔparS) tet, Δspo0J::spec, sacA::hbsu-mcherry kan*	Graham *et al.* 2014	S3
BDR2866	*pelB::Psoj-mgfpmut3-spo0J **R82A** (ΔparS) tet, Δspo0J::spec, sacA::hbsu-mcherry kan*	Graham *et al.* 2014	S3
BLS005	*pelB::Psoj-mgfpmut3-spo0J **H57E** (ΔparS) tet, Δspo0J::spec, sacA::hbsu-mcherry kan*	This work	S3
BLS007	*pelB::Psoj-mgfpmut3-spo0J **L60E** (ΔparS) tet,*	This work	2, S3

Strain	Genotype	Source	Figure
	Δspo0J::spec, sacA::hbsu-mcherry kan		
BLS008	*pelB::Psoj-mgfpmut3-spo0J* ***R39A*** *(ΔparS) tet, Δspo0J::spec, sacA::hbsu-mcherry kan*	This work	2, S3
BLS014	*pelB::Psoj-mgfpmut3-spo0J* ***Q140A*** *(ΔparS) tet, Δspo0J::spec, sacA::hbsu-mcherry kan*	This work	2, S3
BLS015	*pelB::Psoj-mgfpmut3-spo0J* ***Q61A*** *(ΔparS) tet, Δspo0J::spec, sacA::hbsu-mcherry kan*	This work	S3
BLS016	*pelB::Psoj-mgfpmut3-spo0J* ***R105A*** *(ΔparS) tet, Δspo0J::spec, sacA::hbsu-mcherry kan*	This work	S3
BLS017	*pelB::Psoj-mgfpmut3-spo0J* ***E52R*** *(ΔparS) tet, Δspo0J::spec, sacA::hbsu-mcherry kan*	This work	S5
BLS018	*pelB::Psoj-mgfpmut3-spo0J* ***M104A*** *(ΔparS) tet, Δspo0J::spec, sacA::hbsu-mcherry kan*	This work	2, S3
BLS021	*pelB::Psoj-mgfpmut3-spo0J* ***E78R*** *(ΔparS) tet, Δspo0J::spec, sacA::hbsu-mcherry kan*	This work	2, S4
BLS022	*pelB::Psoj-mgfpmut3-spo0J* ***P62A*** *(ΔparS) tet, Δspo0J::spec, sacA::hbsu-mcherry kan*	This work	S4
BLS024	*pelB::Psoj-mgfpmut3-spo0J* ***N112S*** *(ΔparS) tet, Δspo0J::spec, sacA::hbsu-mcherry kan*	This work	S5
BLS032	*pelB::Psoj-mgfpmut3-spo0J* ***Q61R*** *(ΔparS) tet, Δspo0J::spec, sacA::hbsu-mcherry kan*	This work	S5
BLS033	*pelB::Psoj-mgfpmut3-spo0J* ***I74A*** *(ΔparS) tet, Δspo0J::spec, sacA::hbsu-mcherry kan*	This work	2, S4
BLS034	*pelB::Psoj-mgfpmut3-spo0J* ***V75A*** *(ΔparS) tet, Δspo0J::spec, sacA::hbsu-mcherry kan*	This work	S3
BLS035	*pelB::Psoj-mgfpmut3-spo0J* ***F81A*** *(ΔparS) tet, Δspo0J::spec, sacA::hbsu-mcherry kan*	This work	S3
BLS036	*pelB::Psoj-mgfpmut3-spo0J* ***R105E*** *(ΔparS) tet, Δspo0J::spec, sacA::hbsu-mcherry kan*	This work	2, S3
BLS038	*pelB::Psoj-mgfpmut3-spo0J* ***Y72A*** *(ΔparS) tet, Δspo0J::spec, sacA::hbsu-mcherry kan*	This work	2, S4
BLS045	*pelB::Psoj-mgfpmut3-spo0J* ***Q140R*** *(ΔparS) tet, Δspo0J::spec, sacA::hbsu-mcherry kan*	This work	S3
BLS046	*pelB::Psoj-mgfpmut3-spo0J* ***V75E*** *(ΔparS) tet, Δspo0J::spec, sacA::hbsu-mcherry kan*	This work	2, S4
BLS050	*pelB::Psoj-mgfpmut3-spo0J* ***Q61R + R82A*** *(ΔparS) tet, Δspo0J::spec, sacA::hbsu-mcherry kan*	This work	S20
BLS051	*pelB::Psoj-mgfpmut3-spo0J* ***Q61R + R105E*** *(ΔparS) tet, Δspo0J::spec, sacA::hbsu-mcherry kan*	This work	S20
BLS052	*pelB::Psoj-mgfpmut3-spo0J* ***G77S + R79A*** *(ΔparS) tet, Δspo0J::spec, sacA::hbsu-mcherry kan*	This work	S20
BDR2711	*pelB::Psoj-mgfpmut3-spo0J* ***WT*** *(ΔparS) tet, Δspo0J::spec*	Graham *et al.* 2014	S2
BDR2709	*pelB::Psoj-mgfpmut3-spo0J* ***G77S*** *(ΔparS) tet, Δspo0J::spec*	Graham *et al.* 2014	S2
BDR2710	*pelB::Psoj-mgfpmut3-spo0J* ***R79A*** *(ΔparS) tet, Δspo0J::spec*	Graham *et al.* 2014	S2
BDR2713	*pelB::Psoj-mgfpmut3-spo0J* ***R80A*** *(ΔparS) tet, Δspo0J::spec*	Graham *et al.* 2014	S2
BDR2849	*pelB::Psoj-mgfpmut3-spo0J* ***R82A*** *(ΔparS) tet, Δspo0J::spec*	Graham *et al.* 2014	S2
BLS001	*pelB::Psoj-mgfpmut3-spo0J* ***H57E*** *(ΔparS) tet, Δspo0J::spec*	This work	S2
BLS003	*pelB::Psoj-mgfpmut3-spo0J* ***L60E*** *(ΔparS) tet,*	This work	S2

Strain	Genotype	Source	Figure
	Δspo0J::spec		
BLS004	*pelB::Psoj-mgfpmut3-spo0J* ***R39A*** *(ΔparS) tet, Δspo0J::spec*	This work	S2
BLS009	*pelB::Psoj-mgfpmut3-spo0J* ***Q140A*** *(ΔparS) tet, Δspo0J::spec*	This work	S2
BLS010	*pelB::Psoj-mgfpmut3-spo0J* ***Q61A*** *(ΔparS) tet, Δspo0J::spec*	This work	S2
BLS011	*pelB::Psoj-mgfpmut3-spo0J* ***R105A*** *(ΔparS) tet, Δspo0J::spec*	This work	S2
BLS012	*pelB::Psoj-mgfpmut3-spo0J* ***E52R*** *(ΔparS) tet, Δspo0J::spec*	This work	S2
BLS013	*pelB::Psoj-mgfpmut3-spo0J* ***M104A*** *(ΔparS) tet, Δspo0J::spec*	This work	S2
BLS019	*pelB::Psoj-mgfpmut3-spo0J* ***E78R*** *(ΔparS) tet, Δspo0J::spec*	This work	S2
BLS020	*pelB::Psoj-mgfpmut3-spo0J* ***P62A*** *(ΔparS) tet, Δspo0J::spec*	This work	S2
BLS027	*pelB::Psoj-mgfpmut3-spo0J* ***Q61R*** *(ΔparS) tet, Δspo0J::spec*	This work	S2
BLS028	*pelB::Psoj-mgfpmut3-spo0J* ***I74A*** *(ΔparS) tet, Δspo0J::spec*	This work	S2
BLS029	*pelB::Psoj-mgfpmut3-spo0J* ***V75A*** *(ΔparS) tet, Δspo0J::spec*	This work	S2
BLS030	*pelB::Psoj-mgfpmut3-spo0J* ***F81A*** *(ΔparS) tet, Δspo0J::spec*	This work	S2
BLS031	*pelB::Psoj-mgfpmut3-spo0J* ***R105E*** *(ΔparS) tet, Δspo0J::spec*	This work	S2
BLS037	*pelB::Psoj-mgfpmut3-spo0J* ***Y72A*** *(ΔparS) tet, Δspo0J::spec*	This work	S2
BLS043	*pelB::Psoj-mgfpmut3-spo0J* ***Q140R*** *(ΔparS) tet, Δspo0J::spec*	This work	S2
BLS044	*pelB::Psoj-mgfpmut3-spo0J* ***V75E*** *(ΔparS) tet, Δspo0J::spec*	This work	S2
BLS047	*pelB::Psoj-mgfpmut3-spo0J* ***Q61R + R82A*** *(ΔparS) tet, Δspo0J::spec*	This work	S2
BLS048	*pelB::Psoj-mgfpmut3-spo0J* ***Q61R + R105E*** *(ΔparS) tet, Δspo0J::spec*	This work	S2
BLS049	*pelB::Psoj-mgfpmut3-spo0J* ***G77S + R79A*** *(ΔparS) tet, Δspo0J::spec*	This work	S2
TG309	*pelB::Psoj-mgfpmut3-spo0J* ***N112S*** *(ΔparS) tet, Δspo0J::spec*	This work	S2

Supplementary Table S3: Plasmids used in this study

Plasmid	Description	Source
pKM304	His6-SUMO-Spo0J **WT**	Graham *et al.* 2014
pLS021	His6-SUMO-Spo0J **L60E**	This work
pLS022	His6-SUMO-Spo0J **Q61A**	This work
pLS023	His6-SUMO-Spo0J **R39A**	This work
pLS025	His6-SUMO-Spo0J **R105A**	This work
pLS032	His6-SUMO-Spo0J **M104A**	This work
pLS034	His6-SUMO-Spo0J **E52R**	This work
pLS035	His6-SUMO-Spo0J **P62A**	This work

Plasmid	Description	Source
pLS036	His6-SUMO-Spo0J **Q140A**	This work
pLS037	His6-SUMO-Spo0J **E78R**	This work
pLS038	His6-SUMO-Spo0J **H57E**	This work
pLS055	His6-SUMO-Spo0J **R105E**	This work
pLS057	His6-SUMO-Spo0J **F81A**	This work
pLS061	His6-SUMO-Spo0J **Q140R**	This work
pLS062	His6-SUMO-Spo0J **V75E**	This work
pLS066	His6-SUMO-Spo0J **Q61R + R82A**	This work
pLS067	His6-SUMO-Spo0J **Q61R + R105E**	This work
pLS068	His6-SUMO-Spo0J **G77S + R79A**	This work
pTG037	His6-SUMO-Spo0J **R80A**	Graham *et al.* 2014
pTG052	His6-SUMO-Spo0J **G77S**	Graham *et al.* 2014
pTG105	His6-SUMO-Spo0J **N112S**	This work
pTG114	His6-SUMO-Spo0J **Y72A**	This work
pTG115	His6-SUMO-Spo0J **I74A**	This work
pTG116	His6-SUMO-Spo0J **V75A**	This work
pTG118	His6-SUMO-Spo0J **R79A**	Graham *et al.* 2014
pTG119	His6-SUMO-Spo0J **R82A**	Graham *et al.* 2014
pTG240	His6-SUMO-Spo0J **Q61R**	This work
pWX563	*pelB::Psoj-mgfpmut3-spo0J **WT** (ΔparS) tet*	Graham *et al.* 2014
pLS039	*pelB::Psoj-mgfpmut3-spo0J **H57E** (ΔparS) tet*	This work
pLS041	*pelB::Psoj-mgfpmut3-spo0J **L60E** (ΔparS) tet*	This work
pLS042	*pelB::Psoj-mgfpmut3-spo0J **R39A** (ΔparS) tet*	This work
pLS043	*pelB::Psoj-mgfpmut3-spo0J **Q140A** (ΔparS) tet*	This work
pLS044	*pelB::Psoj-mgfpmut3-spo0J **Q61A** (ΔparS) tet*	This work
pLS045	*pelB::Psoj-mgfpmut3-spo0J **R105A** (ΔparS) tet*	This work
pLS046	*pelB::Psoj-mgfpmut3-spo0J **E52R** (ΔparS) tet*	This work
pLS047	*pelB::Psoj-mgfpmut3-spo0J **M104A** (ΔparS) tet*	This work
pLS048	*pelB::Psoj-mgfpmut3-spo0J **E78R** (ΔparS) tet*	This work
pLS049	*pelB::Psoj-mgfpmut3-spo0J **P62A** (ΔparS) tet*	This work
pLS050	*pelB::Psoj-mgfpmut3-spo0J **Q61R** (ΔparS) tet*	This work
pLS051	*pelB::Psoj-mgfpmut3-spo0J **I74A** (ΔparS) tet*	This work
pLS052	*pelB::Psoj-mgfpmut3-spo0J **V75A** (ΔparS) tet*	This work
pLS053	*pelB::Psoj-mgfpmut3-spo0J **F81A** (ΔparS) tet*	This work
pLS054	*pelB::Psoj-mgfpmut3-spo0J **R105E** (ΔparS) tet*	This work
pLS056	*pelB::Psoj-mgfpmut3-spo0J **Y72A** (ΔparS) tet*	This work
pLS059	*pelB::Psoj-mgfpmut3-spo0J **Q140R** (ΔparS) tet*	This work
pLS060	*pelB::Psoj-mgfpmut3-spo0J **V75E** (ΔparS) tet*	This work
pLS063	*pelB::Psoj-mgfpmut3-spo0J **Q61R + R82A** (ΔparS) tet*	This work
pLS064	*pelB::Psoj-mgfpmut3-spo0J **Q61R + R105E** (ΔparS) tet*	This work
pLS065	*pelB::Psoj-mgfpmut3-spo0J **G77S + R79A** (ΔparS) tet*	This work
pTG138	*pelB::Psoj-mgfpmut3-spo0J **G77S** (ΔparS) tet*	Graham *et al.* 2014
pTG140	*pelB::Psoj-mgfpmut3-spo0J **R79A** (ΔparS) tet*	Graham *et al.* 2014
pTG141	*pelB::Psoj-mgfpmut3-spo0J **R80A** (ΔparS) tet*	Graham *et al.* 2014
pTG142	*pelB::Psoj-mgfpmut3-spo0J **R82A** (ΔparS) tet*	Graham *et al.* 2014
pTG184	*pelB::Psoj-mgfpmut3-spo0J **N112S** (ΔparS) tet*	This work

Supplementary Table S4: Oligonucleotides used in this study

Oligo	Sequence	Use
oLS032F	gagcagccgcttatcgtcagaaa	pLS021; pLS041
oLS031R	aatgccatgctgcagcac	pLS021; pLS041
oLS033F	gcgccgcttatcgtcagaaaatctttaaaag	pLS022; pLS044

Oligo	Sequence	Use
oLS034R	aagaatgccatgctgcagc	pLS022; pLS044
oLS039F	gcggaaattgctttattagaaaaccttcagcg	pLS025
oLS040R	cattaacgcctctgataattcacgg	pLS025
oLS058F	gagggcattcttcagccgcttat	pLS038; pLS039
oLS029R	ctgcagcacagattcttttagttc	pLS038; pLS039
oLS052F	gcgagggaaattgctttattagaa	pLS032; pLS047
oLS052R	taacgcctctgataattcacggac	pLS032; pLS047
oLS054F	cggtctgtgctgcagcatggcatt	pLS034
oLS053R	ttttagttcagctaatgcctcgtc	pLS034
oLS055F	gcgcttatcgtcagaaaatcttta	pLS035; pLS049
oLS055R	ctgaagaatgccatgctgcagca	pLS035; pLS049
oLS056F	cggcggcgttttcgagcg	pLS037; pLS048
oLS056R	acccgcaacaatatcatagccttt	pLS037; pLS048
oLS057F	gcgcttgccaaacgtcttgggaaa	pLS036
oLS057R	ctcttgtgtgagatctaagtgttt	pLS036
oLS063F	aatccttatcagccagcaaaacactttgatgac	pLS023; pLS042
oLS063R	gtcatcaaagtgttttgctggctgataaggatt	pLS023; pLS042
oLS065F	gatctcacacaagaggcgcttgccaaacgtctt	pLS043
oLS065R	aagacgtttggcaagcgcctcttgtgtgagatc	pLS043
oLS067F	tcagaggcgttaatggcggaaattgctttatta	pLS047
oLS067R	taataaagcaatttccgccattaacgcctctga	pLS047
oLS068F	ttagctgaactaaaacggtctgtgctgcagcat	pLS046
oLS068R	atgctgcagcacagaccgttttagttcagctaa	pLS046
oLS077F	tcagaggcgttaatggaggaaattgctttatta	pLS054; pLS055; pLS064; pLS067
oLS077R	taataaagcaatttcctccattaacgcctctga	pLS054; pLS055; pLS064; pLS067
oLS080F	gatctcacacaagagcggcttgccaaacgtctt	pLS059; pLS061
oLS080R	aagacgtttggcaagccgctcttgtgtgagatc	pLS059; pLS061
oLS081F	taaaaggctatgatattgaggcgggtgaacggcgt	pLS060; pLS062
oLS081R	acgccgttcacccgcctcaatatcatagcctttta	pLS060; pLS062
oLS082F	gatattgttgcgagtgaagcgcgttttcgagcg	pLS065; pLS068
oLS082R	cgctcgaaaacgcgcttcactcgcaacaatatc	pLS065; pLS068
oTG027F	gttgcgggtgaacgggcttttcgagcggcaaag	pTG037; pTG141
oTG027R	ctttgccgctcgaaaagcccgttcacccgcaac	pTG037; pTG141
oTG049F	tatgatattgttgcgagtgaacggcgttttc	pTG052; pTG138
oTG049R	gaaaacgccgttcactcgcaacaatatcata	pTG052; pTG138
oTG143	attgctttattagaaagccttcagcgtgaagat	pTG105; pTG184
oTG144	atcttcacgctgaaggctttctaataaagcaat	pTG105; pTG184
oTG159	gaaaatctttaaaaggcgctgatattgttgcgggt	pTG114; pLS056
oTG160	acccgcaacaatatcagcgccttttaaagattttc	pTG114; pLS056
oTG161	ctttaaaaggctatgatgctgttgcgggtgaacgg	pTG115; pLS051
oTG162	ccgttcacccgcaacagcatcatagccttttaaag	pTG115; pLS051
oTG163	taaaaggctatgatattgctgcgggtgaacggcgt	pTG116; pLS052
oTG164	acgccgttcacccgcagcaatatcatagccttta	pTG116; pLS052
oTG167	attgttgcgggtgaagcgcgttttcgagcggca	pTG118; pTG140
oTG168	tgccgctcgaaaacgcgcttcacccgcaacaat	pTG118; pTG140
oTG169	ggtgaacggcgttttgcagcggcaaagctggca	pTG119; pTG142; pLS063; pLS066
oTG170	tgccagctttgccgctgcaaaacgccgttcacc	pTG119; pTG142; pLS063; pLS066
oTG211	gcgggtgaacggcgtgctcgagcggcaaagctg	pLS053; pLS057
oTG223	cagctttgccgctcgagcacgccgttcacccgc	pLS053; pLS057
oTG379	cagcatggcattcttcggccgcttatcgtcaga	pTG240; pLS050
oTG380	tctgacgataagcggccgaagaatgccatgctg	pTG240; pLS050
oTG004R	gcactcgagttatgattctcgttcagacaaaagctc	sequencing

Oligo	Sequence	Use
oTG237	atggctaaaggccttggaa	sequencing
oTG489	TGAGGGATATCGAATTCCTGCAGGCgctatt cctcgagggaggtgtc	single-molecule PIFE (first round of PCR amplification)
oTG491	GACGCGAATTATTTTTGATGGCGggatctgcc gcactgatctca	single-molecule PIFE (first round of PCR amplification)
oTG437	/5Biosg/TGAGGGATATCGAATTCCTGCAG GC	single-molecule PIFE (second round of PCR amplification)
oTG488	/5DigN/GACGCGAATTATTTTTGATGGCG	single-molecule PIFE (second round of PCR amplification)
oLS044F	agaatgttccacgtgaaacaaaga	EMSA (24-bp *parS*)
oLS044R	tctttgtttcacgtggaacattct	EMSA (24-bp *parS*)
oLS046F	agaacgtgcccagggagacaaaga	EMSA (24-bp scrambled *parS*)
oLS046R	tcttgcacgggtccctctgtttct	EMSA (24-bp scrambled *parS*)
oTG041F	cagttgaatcagaatgttccacgtgaaacaaagaaaaaa	EMSA (39-bp *parS*)
oTG041R	ttttttcttgtttcacgtggaacattctgattcaactg	EMSA (39-bp *parS*)
oTG043F	cagttgaatctgacaaatgactaacaatgagagcaaaaa	EMSA (39-bp scrambled *parS*)
oTG043R	tttttgctctcattgttagtcatttgtcagattcaactg	EMSA (39-bp scrambled *parS*)

- All oligonucleotides were obtained from Integrated DNA Technologies (IDT) and the sequences are given in the 5' – 3' direction.
- Capitalized text in oTG489 and oTG491 indicates adapter sequences that are complementary to oTG437 and oTG488, respectively.
- Red text in oLS044F, oLS044R, oTG041F and oTG041R indicates *parS* sequence.

Modifications:

/5Biosg/ - 5' biotin
/5DigN/ - 5' digoxigenin

SUPPLEMENTARY FIGURE LEGENDS

Figure S1. Sequence alignment between ParB homologs. Alignment was generated using Clustal Omega with ParB sequences from *Bacillus subtilis* (*Bs*Spo0J), *Helicobacter pylori* (*Hp*Spo0J), *Thermus thermophilus* (*Th*Spo0J), *Caulobacter crescentus* (*Cc*ParB), *Pseudomonas aeruginosa* (*Pa*ParB), *Streptococcus pneumoniae* (*Sp*ParB), *Vibrio cholerae* chromosome I (*Vc*ParB), RP4 plasmid (RP4KorB) and *Enterobacteria* phage P1 (P1ParB). ParB Box I (S53 – R66 in *Bs*Spo0J) and Box II (Y72 – A83 in *Bs*Spo0J) are marked. Colours indicate levels of conservation. Arrows on the bottom of the alignment indicate selected residues in the mutagenesis: arrows in magenta and black indicate hubs and interacting residues, respectively, in the 2D network map as shown in Figure 1F. Asterisks indicate residues previously identified to be essential for ParB spreading in *B. subtilis*: G77 (Breier and Grossman 2007), R79 (Graham *et al*. 2014), R80 (Autret *et al.* 2001), and R82 (Graham *et al*. 2014).

Figure S2. Immunoblot analysis of fluorescent protein fusions to *Bs*Spo0J variants. All fusion proteins are intact and expressed at similar levels. Strain PY79 expresses endogenous wild type *Bs*Spo0J without a fluorescent tag. mGFPmut3-*Bs*Spo0J was detected using anti-GFP antibodies and the predicted size of free GFP is indicated (arrowhead). σ^A levels are shown as a control for loading.

Figure S3. Localization of mGFPmut3-tagged *Bs*Spo0J Group I mutants (see Table 2). Some panels are duplicated here from Figure 2 to facilitate comparison. Nucleoid (false-coloured red) was labelled with HBsu-mCherry. Scale bar = 5 μm.

Figure S4. Localization of mGFPmut3-tagged *Bs*Spo0J Group II mutants (see Table 2). Some panels are duplicated here from Figure 2 to facilitate comparison. Nucleoid (false-coloured red) was labelled with HBsu-mCherry. Scale bar = 5 μm.

Figure S5. Localization of mGFPmut3-tagged *Bs*Spo0J Group III mutants (see Table 2). Images for the wild type are duplicated here from Figure 2 to facilitate comparison. Nucleoid (false-coloured red) was labelled with HBsu-mCherry. Scale bar = 5 μm.

Figure S6. Interaction between H67 and E88 in the *Hp*Spo0J-*parS* complex. (**A**) Cartoon representation of the C-terminally truncated *Hp*Spo0J-*parS* crystal structure (Chen *et al.* 2015) (PDB code: 4UMK). Figure is not drawn to scale. (**B**) Interaction (magenta dashed line) between H67 on chain A (blue) and E88 on chain B (orange) in *trans.* Figure was prepared in PyMOL.

Figure S7. Protein purification of *Bs*Spo0J. (**A**) Coomassie-stained SDS-PAGE gel showing wild type *Bs*Spo0J and mutants purified via His6-SUMO expression system (see Methods). (**B**) Light scattering signals represented in Rayleigh ratio for wild type *Bs*Spo0J (black solid line) and a BSA standard (black dashed line). Signals were monitored using SEC-MALS and normalized to the maximum in each curve. A single peak was observed for wild type *Bs*Spo0J (red solid line) with a calculated molecular weight (MW) of 63.5 ± 0.4 kDa, corresponding to a dimeric protein. Three major peaks with calculated MWs of 62.2 ± 0.3 kDa, 123.6 ± 0.2 kDa, and 201.2 ± 0.6 kDa were observed for BSA (red dashed lines), corresponding to monomeric, dimeric, and higher oligomeric proteins, respectively.

Figure S8. Quantification of the kinetics of DNA compaction by wild type *Bs*Spo0J at 100 nM. (**A**) Trajectories of fold increase in integrated fluorescence intensity (blue) and DNA length (green) of a single Cy3-labelled DNA compacted by wild type *Bs*Spo0J. Time zero was defined as the starting point of protein association. Lag time (t_{lag}) is the time between protein binding and the initiation of DNA compaction. t_{lag} = 5.1 s as shown here. (**B**) Histogram of lag times (t_{lag}) fitted with a Gaussian distribution (red) for wild type *Bs*Spo0J. (**C**) Trajectory of DNA length (green) of a single Cy3-labelled DNA compacted by wild type *Bs*Spo0J. Rate of DNA compaction (k_c) was estimated by linear fitting of the trajectory (red dashed line) between maximum and minimum DNA lengths (purple dashed lines). The slope shown here is 0.44 ± 0.02 μm s^{-1} (fit ± error estimate). (**D**) Histogram of rates of DNA compaction (k_c) fitted with a Gaussian distribution (red) for wild type *Bs*Spo0J.

Figure S9. Single-molecule DNA compaction by *Bs*Spo0J Group I mutants (see Table 2). (**A**) Fold increase in integrated fluorescence intensity and DNA length trajectories for the wild type *Bs*Spo0J (black; reproduced in each panel) and mutants (red) at a protein concentration of 100 nM. Each trajectory was averaged over 20 – 30 DNAs. Some panels are re-plotted here from Figure 3C to facilitate comparison. Note that in comparison to Figure 3C, trajectories shown here were plotted over a longer time scale to capture the complete DNA compaction by mutants. The fold change in integrated intensity showed a decreasing trend after reaching equilibrium due to photobleaching rather than protein dissociation (see part **B**). (**B**) Overlay of a trajectory showing association of *Bs*Spo0J R80A to Cy3-labelled DNAs (red; reproduced from part **A**) and a photobleaching curve of Cy3-labelled DNAs in the absence of protein (blue). Each trajectory was averaged over 20 – 30 DNAs. Integrated fluorescence intensities of Cy3-labelled DNAs were normalized by the maximum values. Plots were aligned at the time point marked by the purple dashed line when the integrated intensity started to decrease.

Figure S10. Group I mutants of *Bs*Spo0J (see Table 2) are defective in DNA compaction even at a higher protein concentration. Fold increase in integrated fluorescence intensity and DNA length trajectories for the wild type *Bs*Spo0J (black; reproduced in each panel) and mutants (red) at a protein concentration of 300 nM. Some compaction activity is observed for the V75A and F81A mutants, consistent with their ability to form wild type-like foci *in vivo* (Supplementary Figure S3). Each trajectory was averaged over 20 – 30 DNAs.

Figure S11. DNA compaction by *Bs*Spo0J mutants in low salt. Fold increase in integrated fluorescence intensity and DNA length trajectories for R80A (blue), R105E (green), or R82A (red) at a protein

concentration of 100 nM in binding buffer containing 50 mM NaCl. Each trajectory was averaged over 20 – 30 DNAs.

Figure S12. Single-molecule DNA compaction by *Bs*Spo0J Group II and Group III mutants (see Table 2). (**A**) Fold increase in integrated fluorescence intensity and DNA length trajectories for the wild type *Bs*Spo0J (black; reproduced in each panel) and mutants (red) at a protein concentration of 100 nM. Each trajectory was averaged over 20 – 30 DNAs. Some panels are re-plotted here from Figure 3C to facilitate comparison. (**B**) Trajectory of the mutant N112S at a protein concentration of 300 nM.

Figure S13. In vitro characterization of the specific binding of *Bs*Spo0J to the 24-bp *parS* DNA duplexes without competitor DNA. Protein concentrations were 0.2, 0.4, 0.8 μM in (**A**) – (**E**), and 0.2, 0.4, 0.8, and 1.0 μM in (**F**) – (**J**). Asterisk and arrow indicate position of the wells and free DNA respectively in each gel. Some panels are duplicated here from Figure 4 to facilitate comparison.

Figure S14. In vitro characterization of the specific binding of *Bs*Spo0J to the 39-bp *parS* DNA duplexes supplemented with cold 39-bp scrambled *parS* competitor DNA. Protein concentrations were 0.2, 0.4, 0.8 μM in (**A**) – (**E**), and 0.2, 0.4, 0.8, and 1.0 μM in (**F**) – (**J**). Asterisk and arrow indicate position of the wells and free DNA respectively in each gel. Some panels are duplicated here from Figure 4 to facilitate comparison.

Figure S15. In vitro characterization of the non-specific binding of *Bs*Spo0J to the 39-bp DNA duplexes containing a scrambled *parS* site. Protein concentrations were 0.2, 0.4, 0.8 μM in (**A**) – (**E**), and 0.2, 0.4, 0.8, and 1.0 μM in (**F**) – (**J**). Asterisk and arrow indicate position of the wells and free DNA respectively in each gel.

Figure S16. Crystal structure of C-terminally truncated *Tt*Spo0J (Leonard *et al.* 2004) (PDB code: 1VZ0). C-terminally truncated*Tt*Spo0J monomers (chain A in magenta and chain B in green) form an antiparallel dimer through interactions between the alpha helix "H2" of one monomer and the globular domain of the other. Dimerization is further stabilized by hydrophobic interactions between the extended N-terminal chain of one monomer and multiple β-sheets of the other at each end of the dimer. The helix-turn-helix DNA-binding domain is highlighted in each monomer for orientation (orange in chain A and yellow in chain B, respectively). Residues affected by Group I and Group III mutations (see Table 2), which are highlighted in red, are not involved in the N-terminal dimerization interface. Residues affected by Group II mutations including P62A (see Table 2), which are highlighted in blue, are involved in stabilizing the N-terminal dimerization. A 180° reverse view of the dimer is shown for comparison. Figure was prepared in PyMOL.

Figure S17. Residues in the highly conserved ParB Box II region coordinate multiple interactions between ParB dimers both in *cis* and in *trans*. (**A**) Cartoon representation of the C-terminally truncated *Hp*Spo0J-*parS* crystal structure (Chen *et al.* 2015) (PDB code: 4UMK). Figure is not drawn to scale. (**B**) Residues R89 and I85 in ParB Box II (shown in yellow) of chain D (green) interact in *cis* with E150 in the helix-turn-helix (HTH) domain (shown in pink) of chain B (orange). Interactions between other residues in ParB Box II (shown in yellow) of chain D (green) and residues on chain B (orange) outside the HTH domain are also displayed. Location of residue P72 on chain D (green) is indicated. (**C**) Multiple interactions in *trans* between chain A (blue) and chain B (orange) coordinated by residues in ParB Box II on each chain (ParB Box II on chain A is shown in cyan and ParB Box II on chain B is shown in yellow). Residues Y82 – E88 (Y72 – E78 in *Bs*Spo0J) in ParB Box II are located on the β-sheet and loop region. Residues R89 – R92 (R79 – R82 in *Bs*Spo0J) in ParB Box II are located on the α-helix. Residue P72 (P62 in *Bs*Spo0J) on chain B (orange) also interacts with L74 on chain A (blue) in *trans*. Yellow dashed lines indicate hydrogen bonds, and magenta dashed lines indicate hydrophobic interactions. Figures were prepared in PyMOL.

Figure S18. Thermal stability of *Bs*Spo0J mutants in Group I (**A**) subgroup A, (**B**) subgroup B, and (**C**) subgroup C (see Table 2). Thermal denaturation curves for wild type *Bs*Spo0J (black dashed line; reproduced in each panel) and mutants (red) were measured with differential scanning fluorimetry at a protein concentration of 100 μg ml^{-1} (see Methods). Fluorescence intensities were normalized to the

maximum in each curve. Only one replicate of each protein is shown. Some data are re-plotted here from Figure 5A to facilitate comparison.

Figure S19. Thermal stability of *Bs*Spo0J (**A**) Group II mutants and (**B**) Group III mutants (see Table 2). Thermal denaturation curves for wild type *Bs*Spo0J (black dashed line; reproduced in each panel) and mutants (red) were measured with differential scanning fluorimetry at a protein concentration of 100 μg ml^{-1} (see Methods). Fluorescence intensities were normalized to the maximum in each curve. Only one replicate of each protein is shown. Some data are re-plotted here from Figure 5A to facilitate comparison.

Figure S20. In vivo and in vitro characterization of *Bs*Spo0J double mutants. (**A**) Localization of mGFPmut3-tagged *Bs*Spo0J double mutants. Nucleoid (false-colored red) was labelled with HBsu-mCherry. Scale bar = 5 μm. (**B**) Fold increase in integrated fluorescence intensity and DNA length trajectories for the wild type *Bs*Spo0J (black; reproduced in each panel) and double mutants (red) at a protein concentration of 100 nM. Each trajectory was averaged over 20 – 30 DNAs. (**C**) Fold increase in integrated fluorescence intensity and DNA length trajectories for the wild type *Bs*Spo0J (black; reproduced in each panel) and mutants (red) at a protein concentration of 300 nM. Each trajectory was averaged over 20 – 30 DNAs. (**D**) EMSA of wild type *Bs*Spo0J and double mutants binding to the 24-bp *parS* DNA duplexes without competitor DNA. Protein concentrations were 0.2, 0.4, 0.8, and 1.0 μM. (**E**) EMSA of wild type *Bs*Spo0J and double mutants binding to the 39-bp *parS* DNA duplexes supplemented with cold 39-bp scrambled *parS* competitor DNA. Protein concentrations were 0.2, 0.4, 0.8, and 1.0 μM. (**F**) EMSA of wild type *Bs*Spo0J and double mutants binding to the 39-bp DNA duplexes containing a scrambled *parS* site. Protein concentrations were 0.2, 0.4, 0.8, and 1.0 μM. Asterisk and arrow in (**D**) – (**F**) indicate position of the wells and free DNA respectively in each gel. (**G**) Thermal denaturation curves for wild type *Bs*Spo0J (black dashed line; reproduced in each panel) and double mutants (red) at a protein concentration of 100 μg ml^{-1} measured with differential scanning fluorimetry (see Methods). Fluorescence intensities were normalized to the maximum in each curve. Only one replicate of each protein is shown.

Figure S21. Summary of mutagenesis results annotated on the 2D network map generated from the crystal structure (see Methods) indicating *cis* (blue) and *trans* (green) interactions within the *Hp*Spo0J-*parS* tetrameric complex (Chen *et al.* 2015). Interactions between residues within the same *Hp*Spo0J monomer are shown in grey. Highly conserved residues that act as hubs for multiple interactions are circled in magenta. Colours indicate different levels of severity in ParB spreading based on the loss of mGFPmut3-*Bs*Spo0J foci after the highlighted residue was mutated (see Supplementary Table S1 and Table 2 for specific mutations). Non-highlighted residues were not included in the mutagenesis studies. Residue number corresponds to that in *Hp*Spo0J.

SUPPLEMENTARY REFERENCES

Autret, S., Nair, R. and Errington, J. (2001) Genetic analysis of the chromosome segregation protein Spo0J of Bacillus subtilis: evidence for separate domains involved in DNA binding and interactions with Soj protein. *Mol Microbiol*, **41**, 743-755.

Breier, A.M. and Grossman, A.D. (2007) Whole-genome analysis of the chromosome partitioning and sporulation protein Spo0J (ParB) reveals spreading and origin-distal sites on the Bacillus subtilis chromosome. *Mol Microbiol*, **64**, 703-718.

Chen, B.W., Lin, M.H., Chu, C.H., Hsu, C.E. and Sun, Y.J. (2015) Insights into ParB spreading from the complex structure of Spo0J and parS. *Proceedings of the National Academy of Sciences of the United States of America*.

Fujita, M. (2000) Temporal and selective association of multiple sigma factors with RNA polymerase during sporulation in Bacillus subtilis. *Genes Cells*, **5**, 79-88.

Graham, T.G., Wang, X., Song, D., Etson, C.M., van Oijen, A.M., Rudner, D.Z. and Loparo, J.J. (2014) ParB spreading requires DNA bridging. *Genes Dev*, **28**, 1228-1238.

Gruber, S. and Errington, J. (2009) Recruitment of condensin to replication origin regions by ParB/SpoOJ promotes chromosome segregation in B. subtilis. *Cell*, **137**, 685-696.

Leonard, T.A., Butler, P.J. and Lowe, J. (2004) Structural analysis of the chromosome segregation protein Spo0J from Thermus thermophilus. *Mol Microbiol*, **53**, 419-432.

Lin, D.C., Levin, P.A. and Grossman, A.D. (1997) Bipolar localization of a chromosome partition protein in Bacillus subtilis. *Proceedings of the National Academy of Sciences of the United States of America*, **94**, 4721-4726.

Rudner, D.Z., Fawcett, P. and Losick, R. (1999) A family of membrane-embedded metalloproteases involved in regulated proteolysis of membrane-associated transcription factors. *Proceedings of the National Academy of Sciences of the United States of America*, **96**, 14765-14770.

Wang, X., Le, T.B., Lajoie, B.R., Dekker, J., Laub, M.T. and Rudner, D.Z. (2015) Condensin promotes the juxtaposition of DNA flanking its loading site in Bacillus subtilis. *Genes Dev*, **29**, 1661-1675.

Youngman, P.J., Perkins, J.B. and Losick, R. (1983) Genetic transposition and insertional mutagenesis in Bacillus subtilis with Streptococcus faecalis transposon Tn917. *Proceedings of the National Academy of Sciences of the United States of America*, **80**, 2305-2309.

SUPPLEMENTARY FIGURES

Supplementary Figure S1

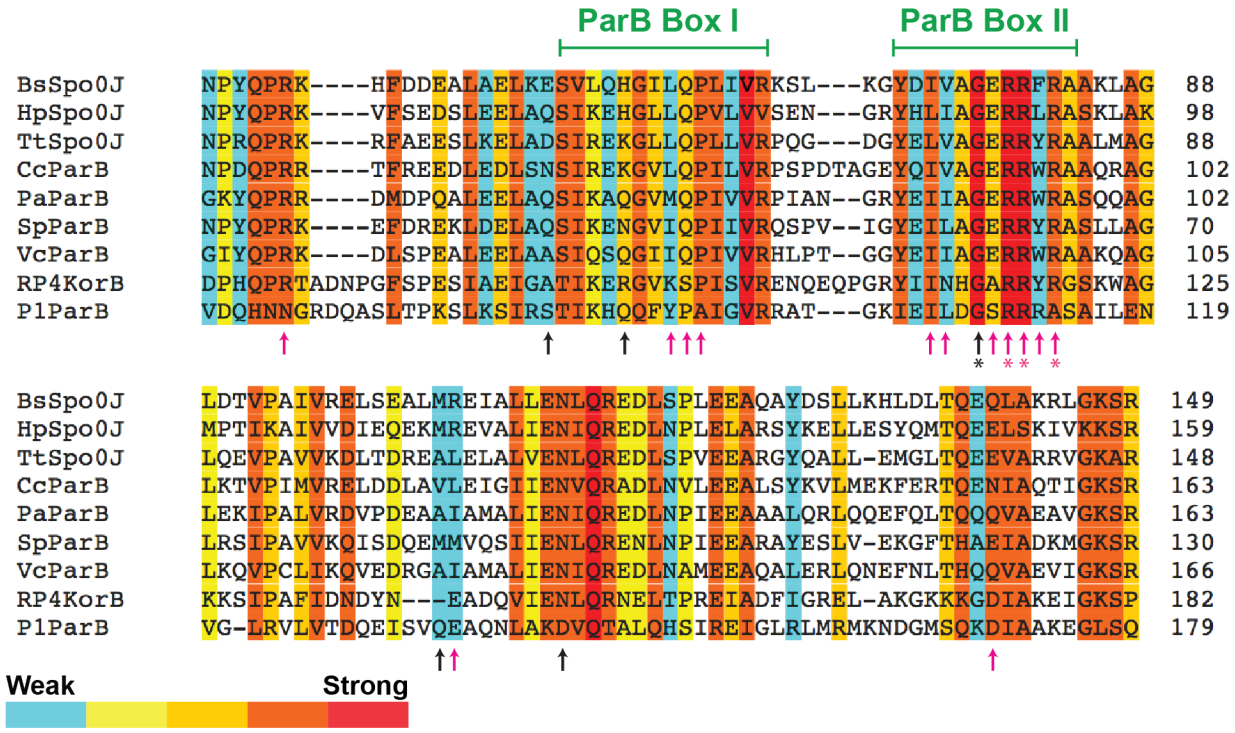

Supplementary Figure S2

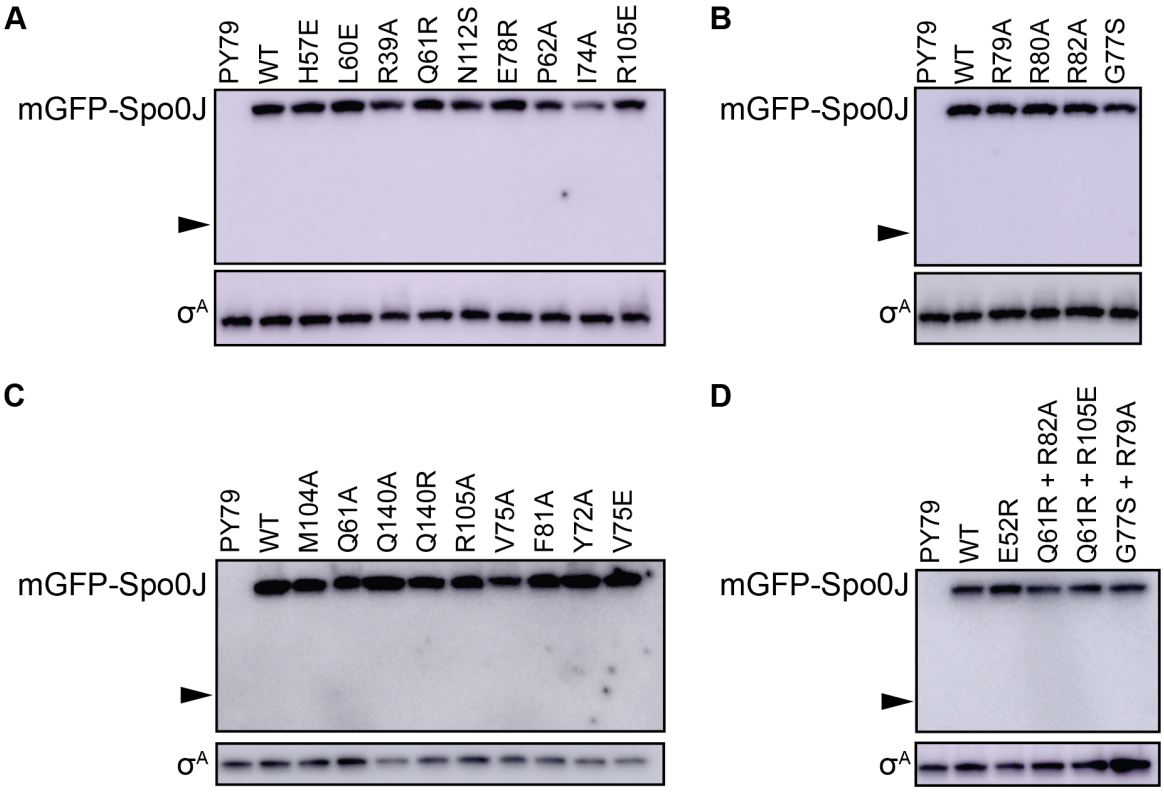

Supplementary Figure S3

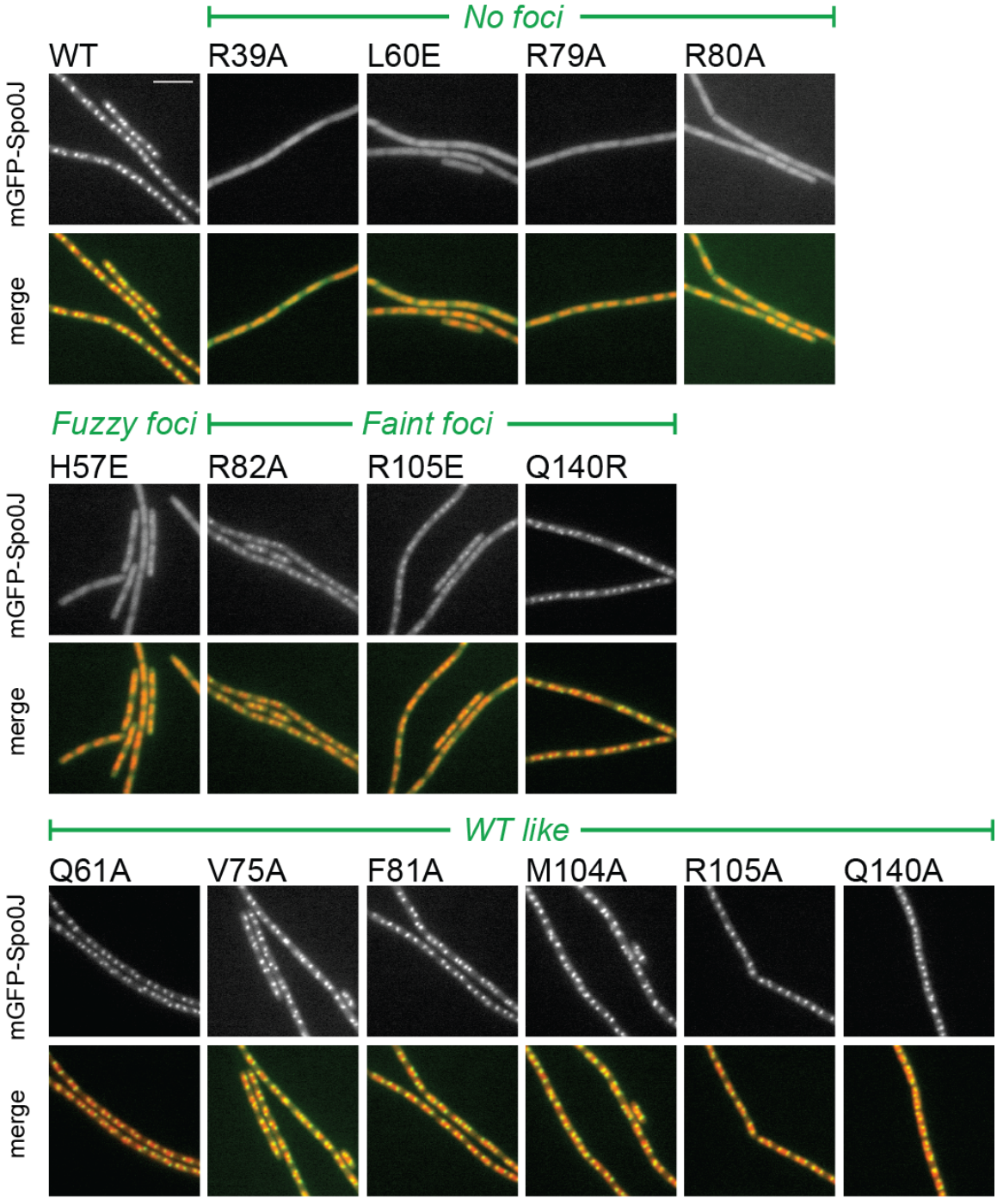

Supplementary Figure S4

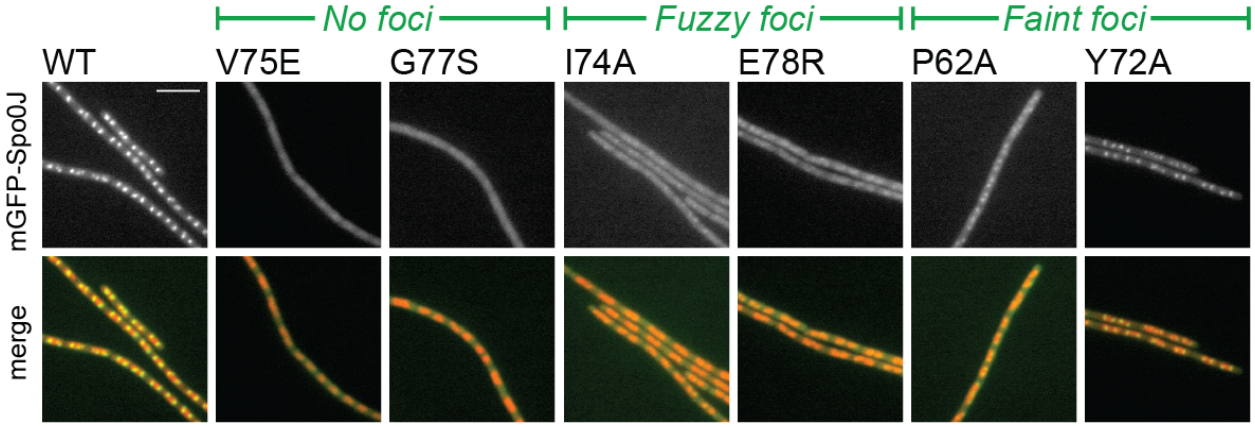

Supplementary Figure S5

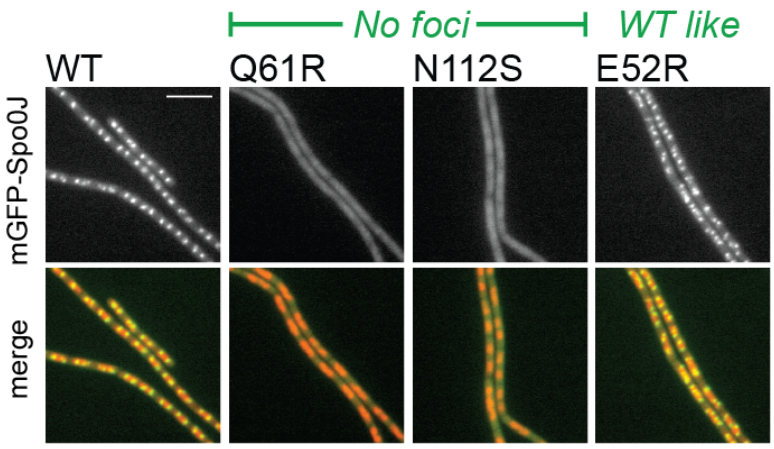

Supplementary Figure S6

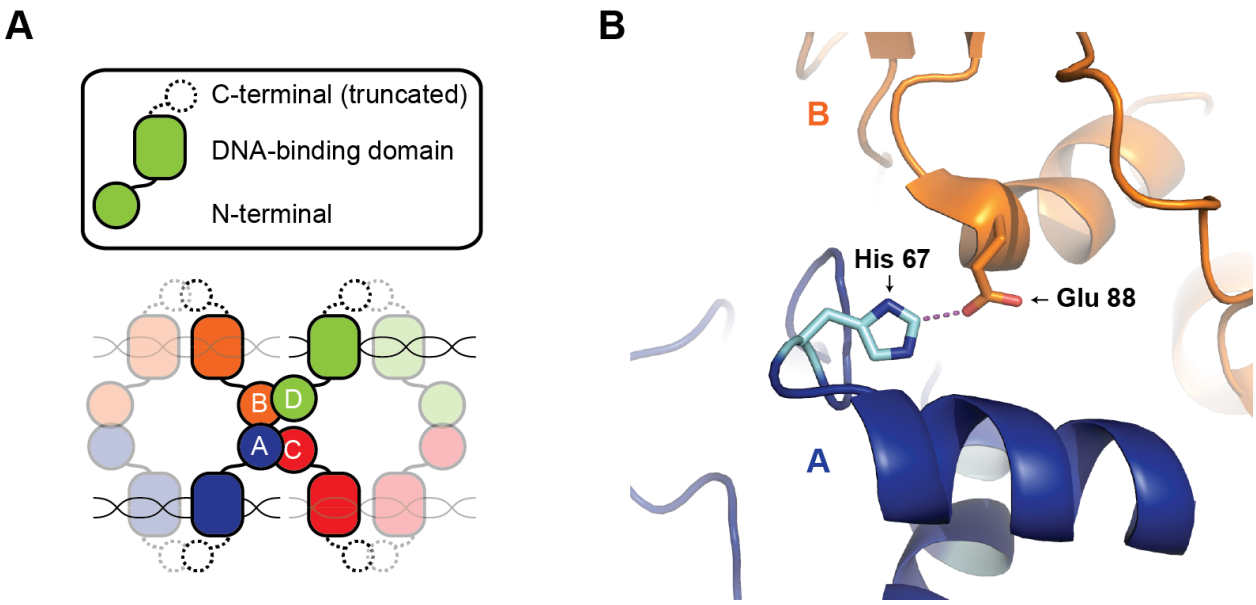

Supplementary Figure S7

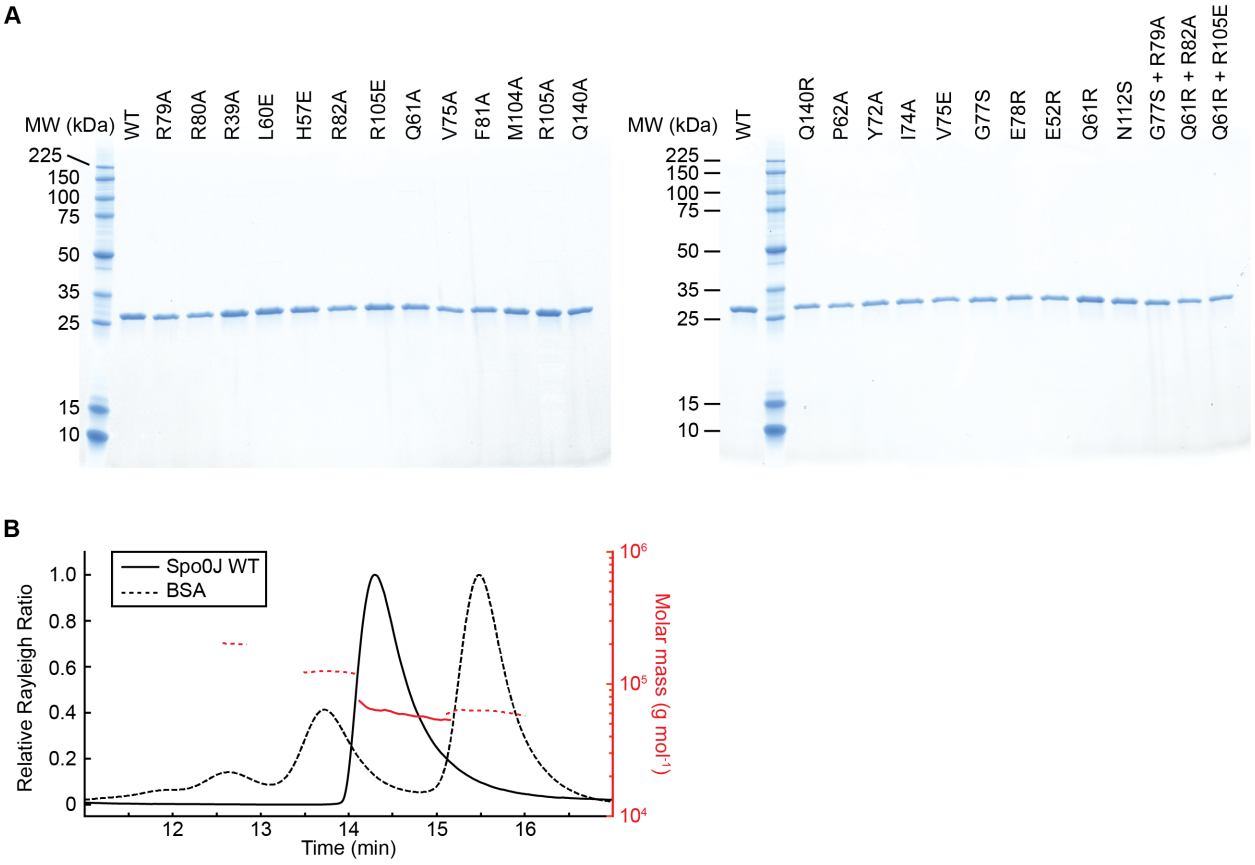

Supplementary Figure S8

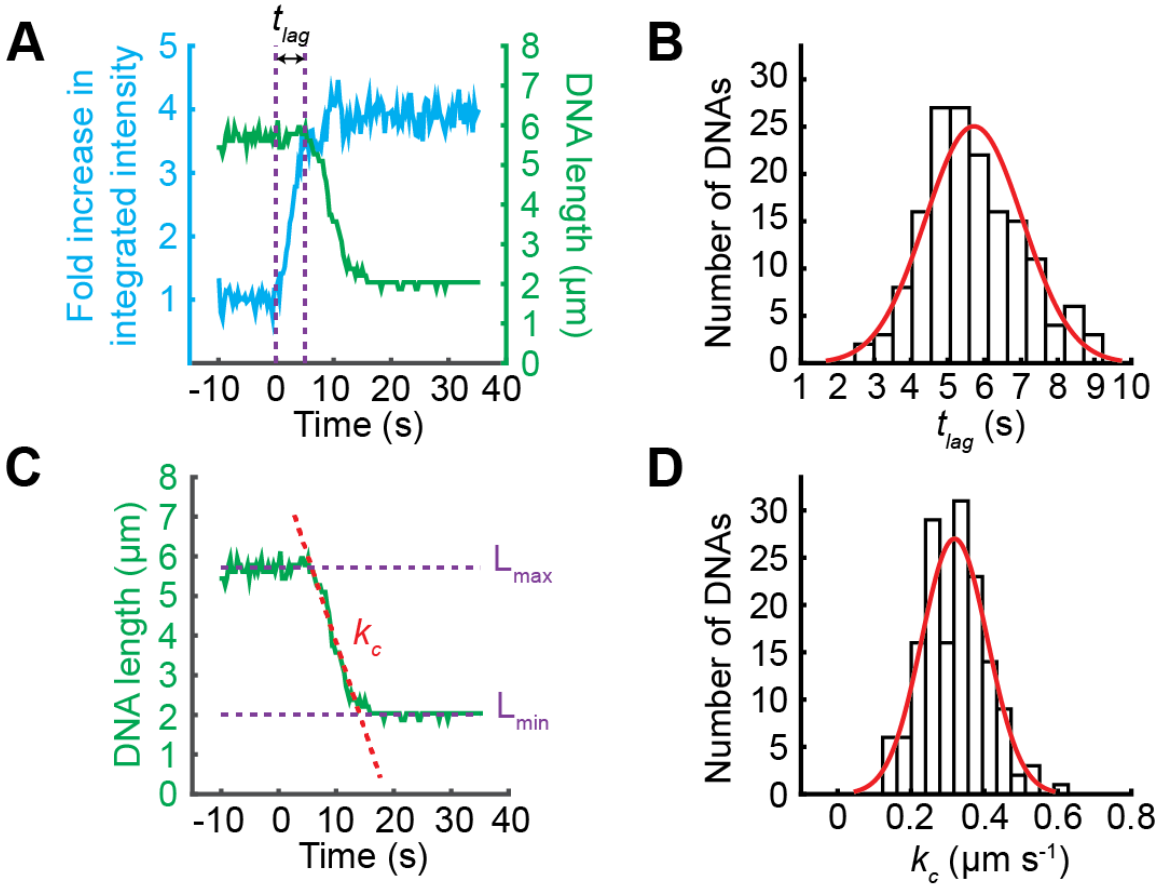

Supplementary Figure S9

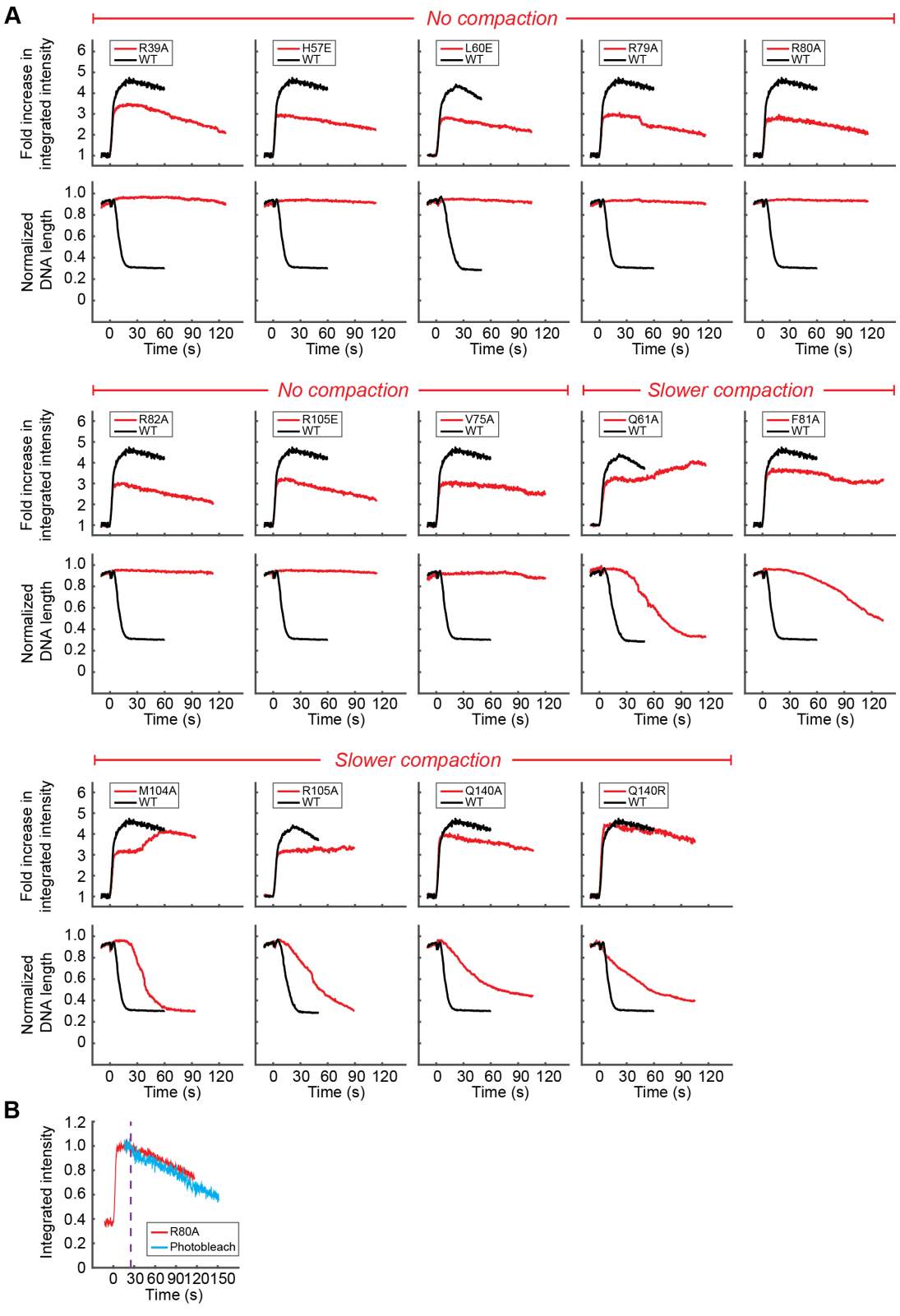

Supplementary Figure S10

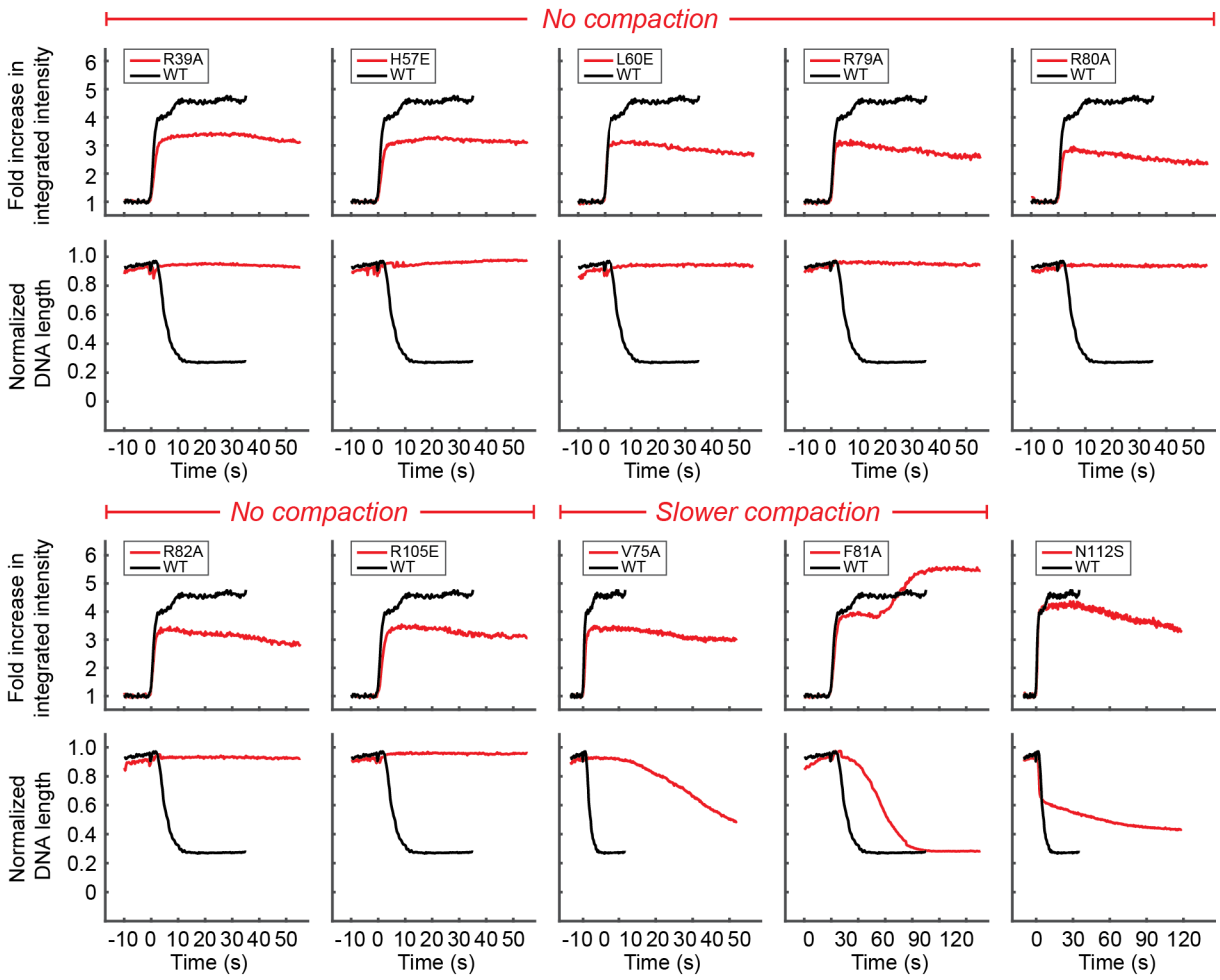

Supplementary Figure S11

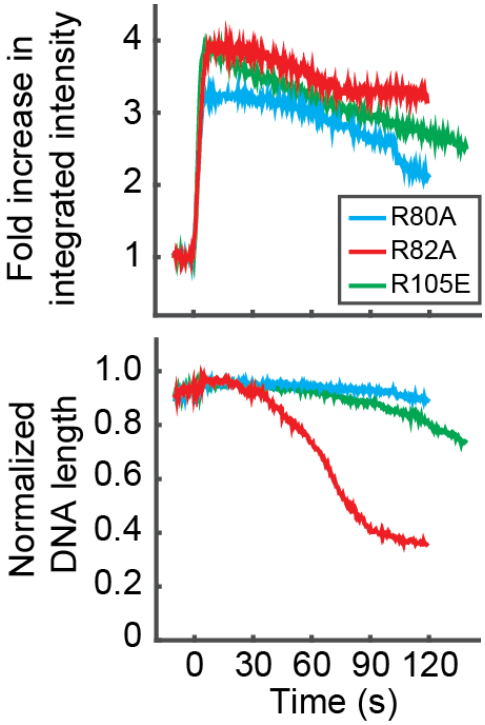

Supplementary Figure S12

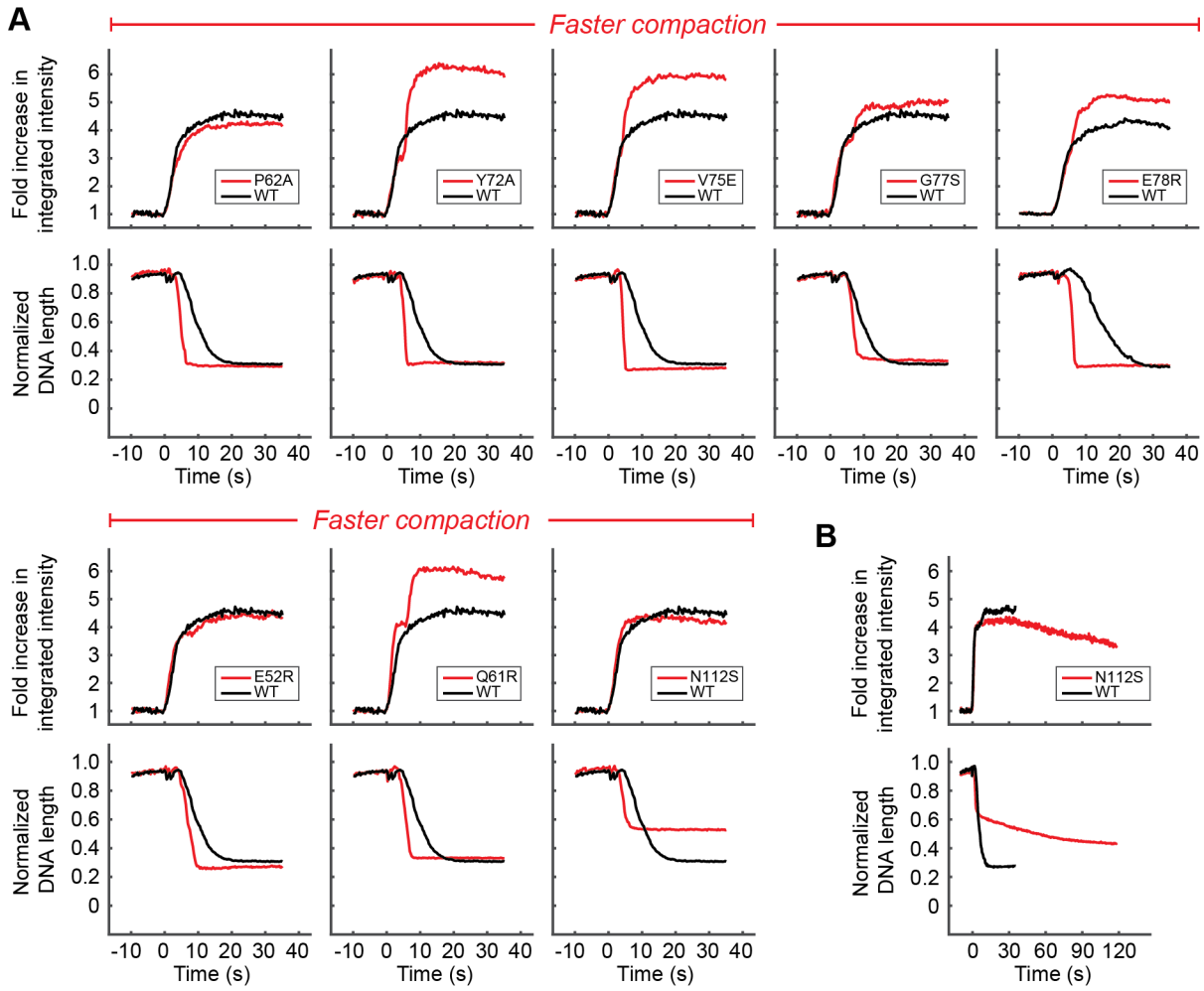

Supplementary Figure S13

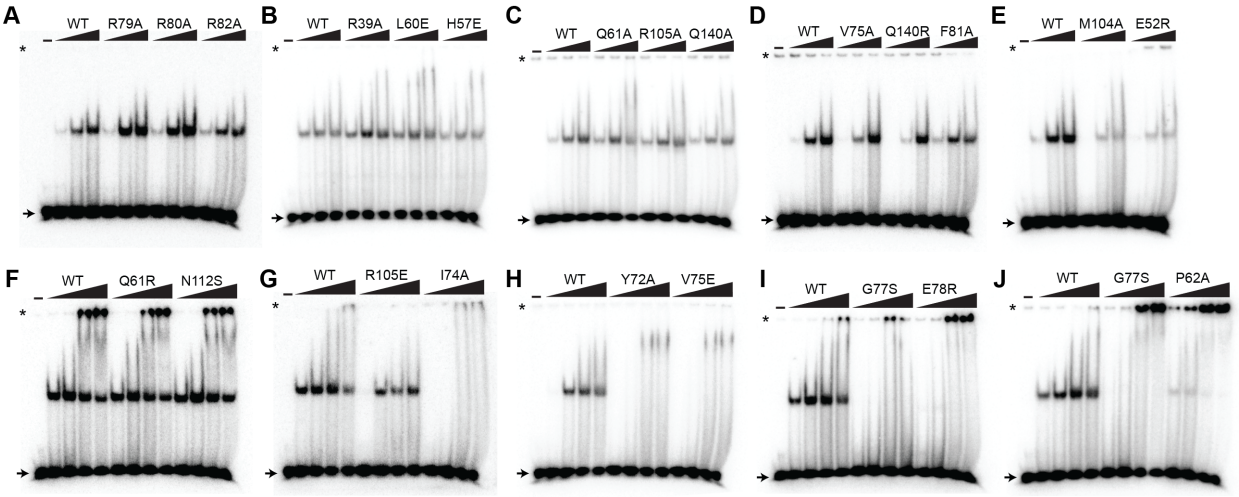

Supplementary Figure S14

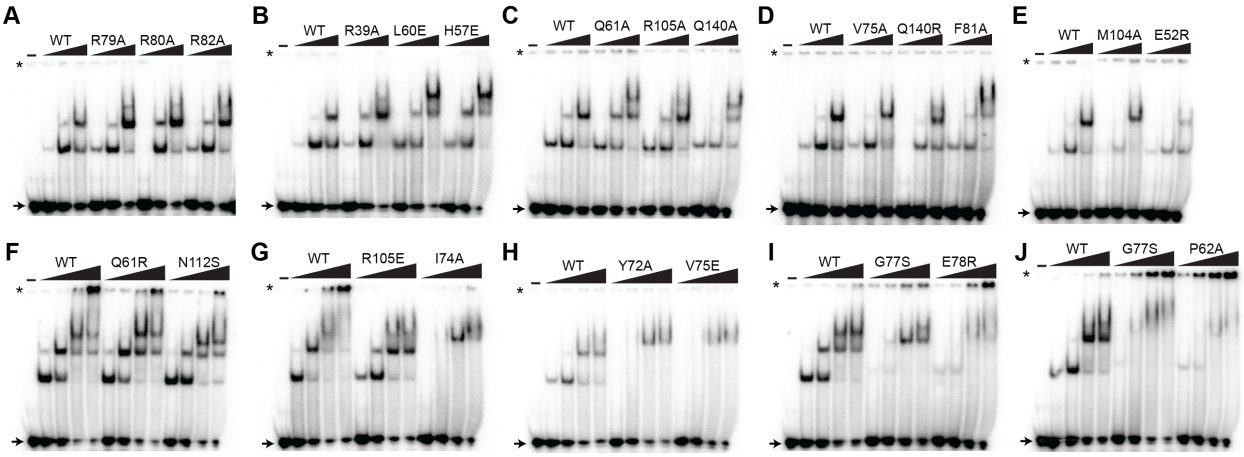

Supplementary Figure S15

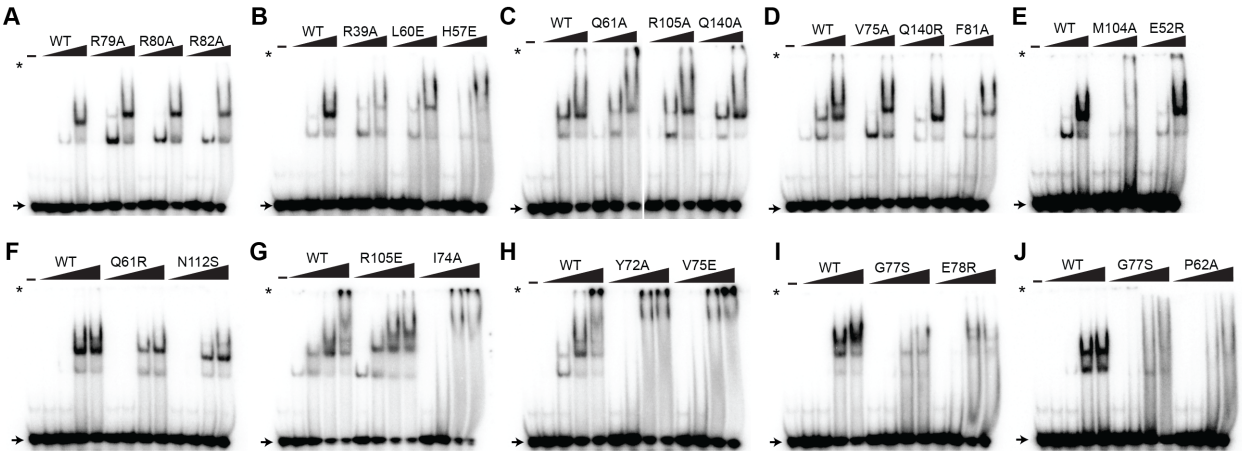

Supplementary Figure S16

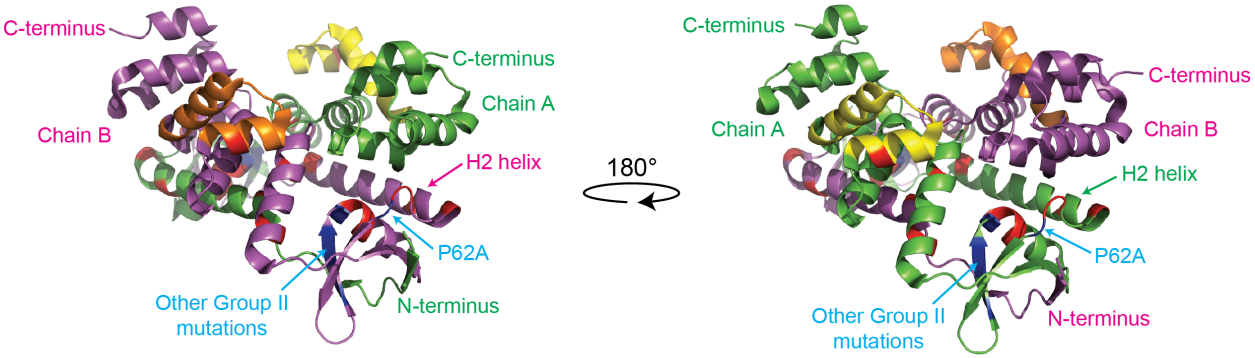

Supplementary Figure S17

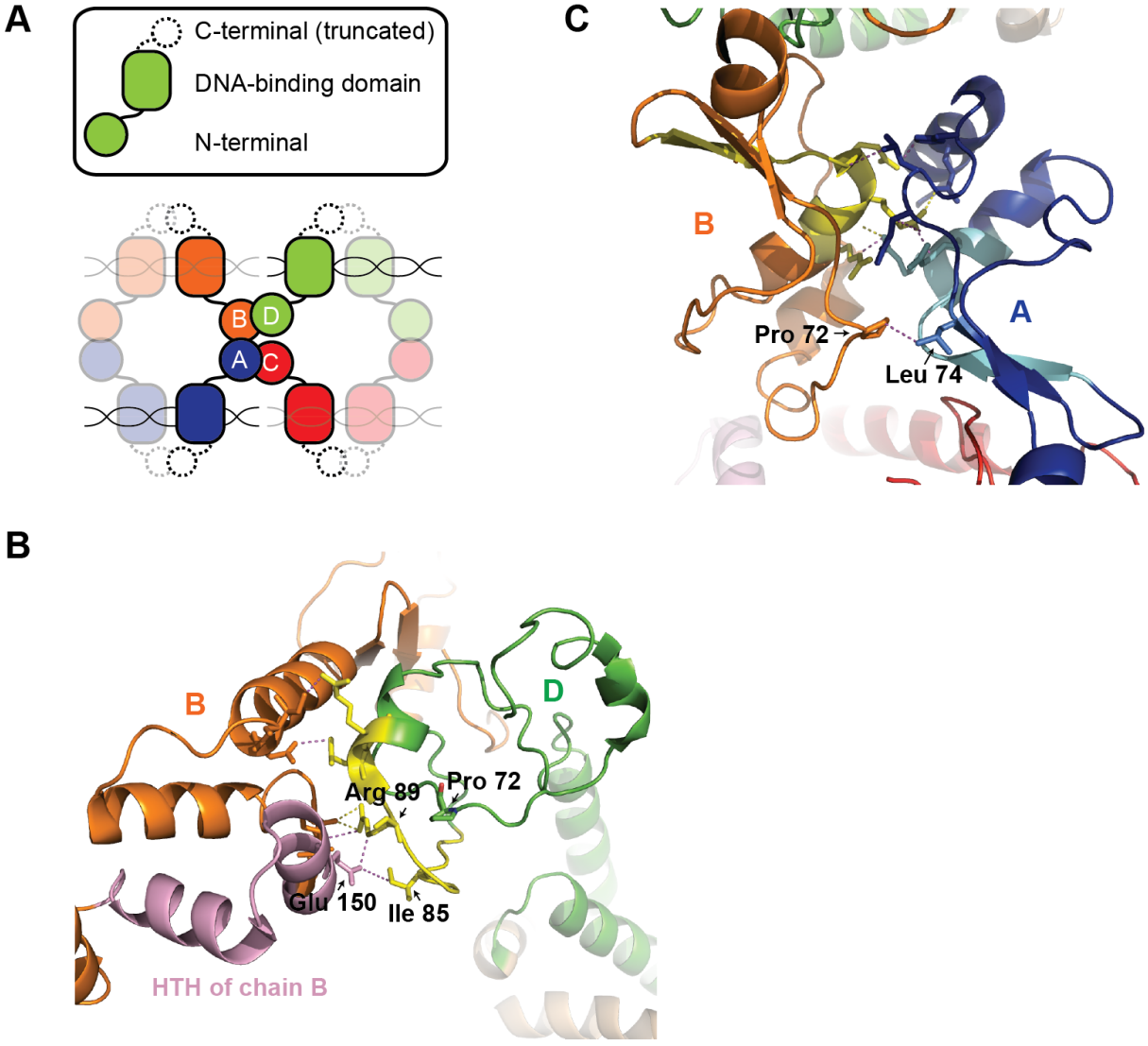

Supplementary Figure S18

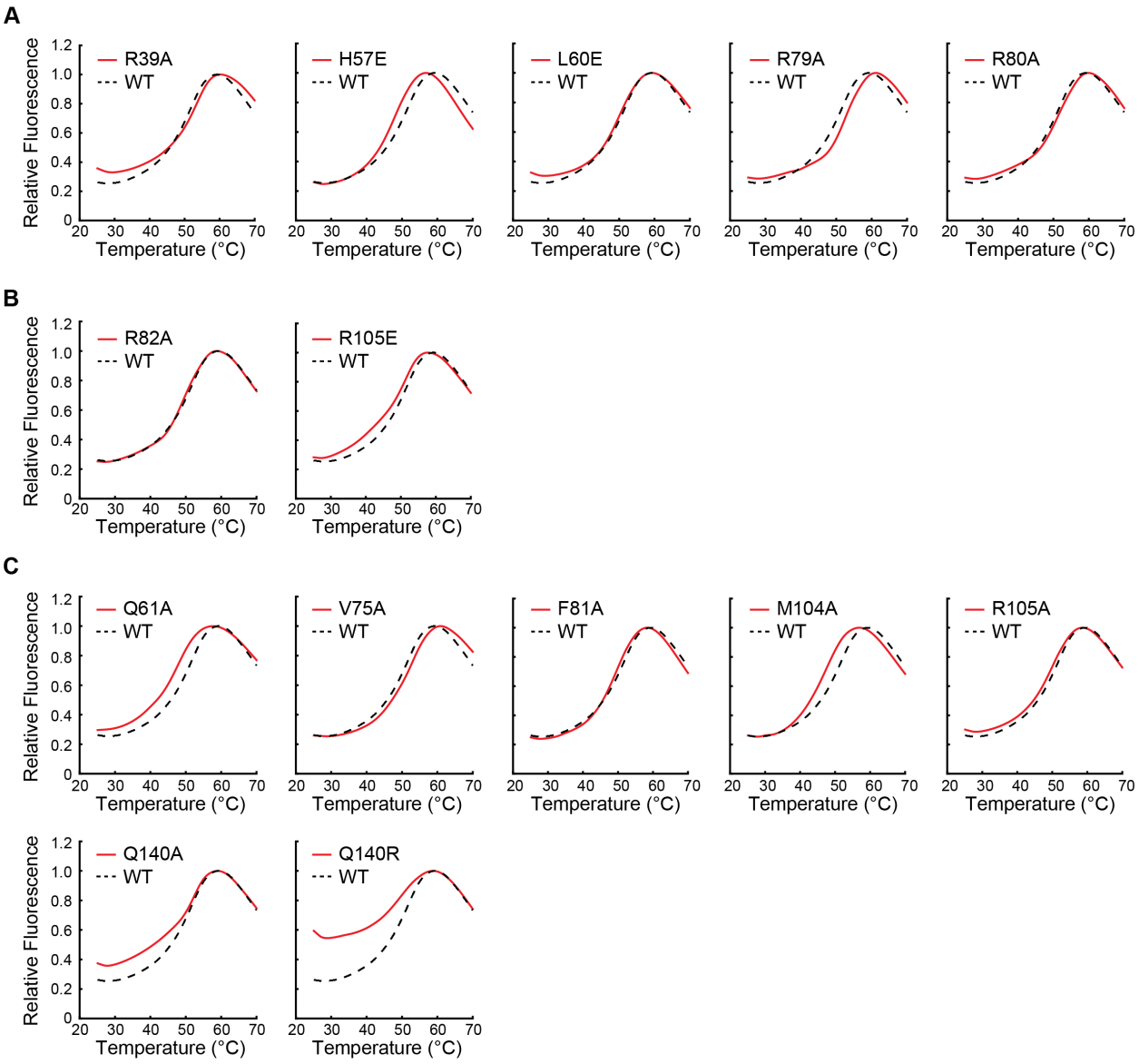

Supplementary Figure S19

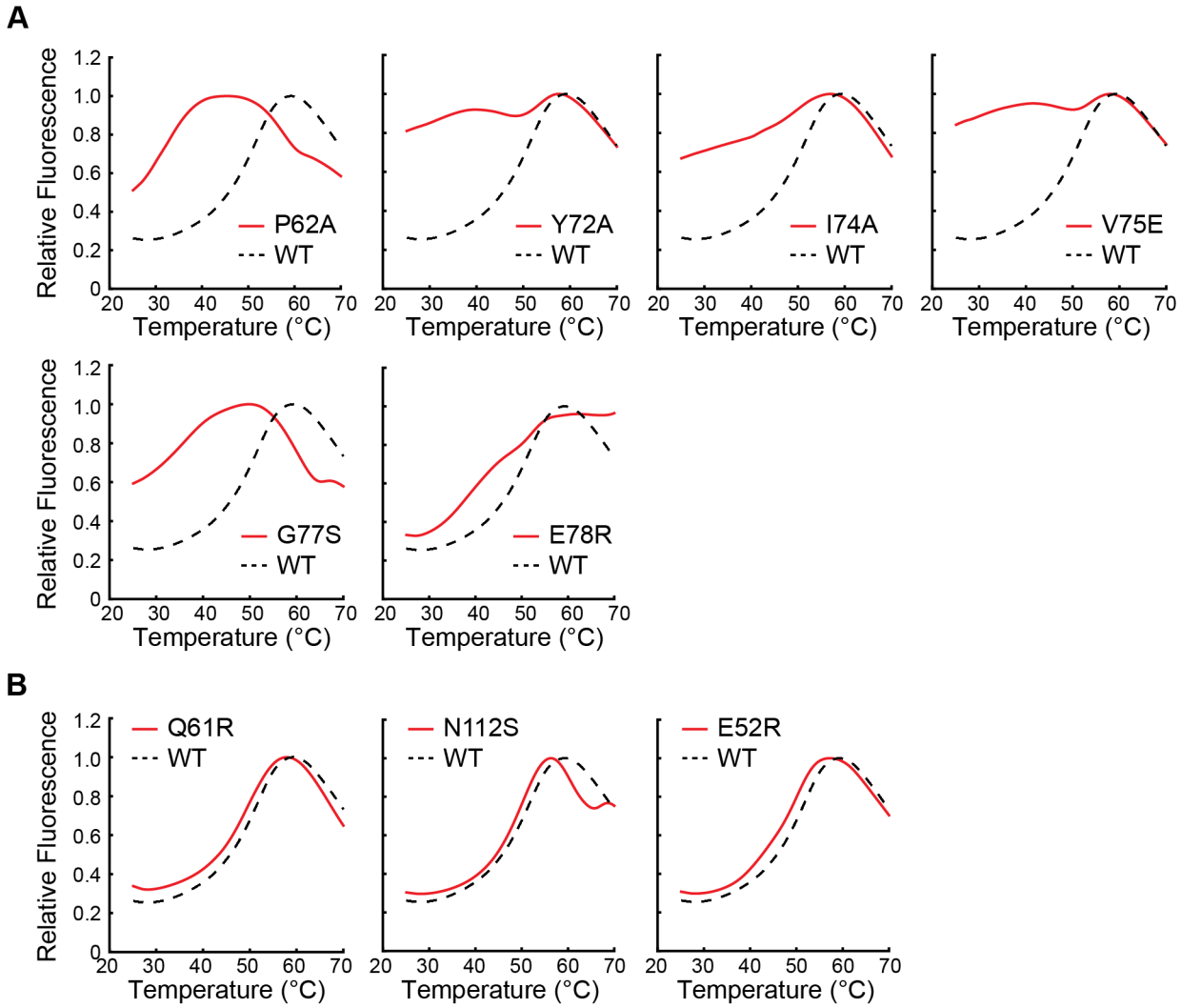

Supplementary Figure S20

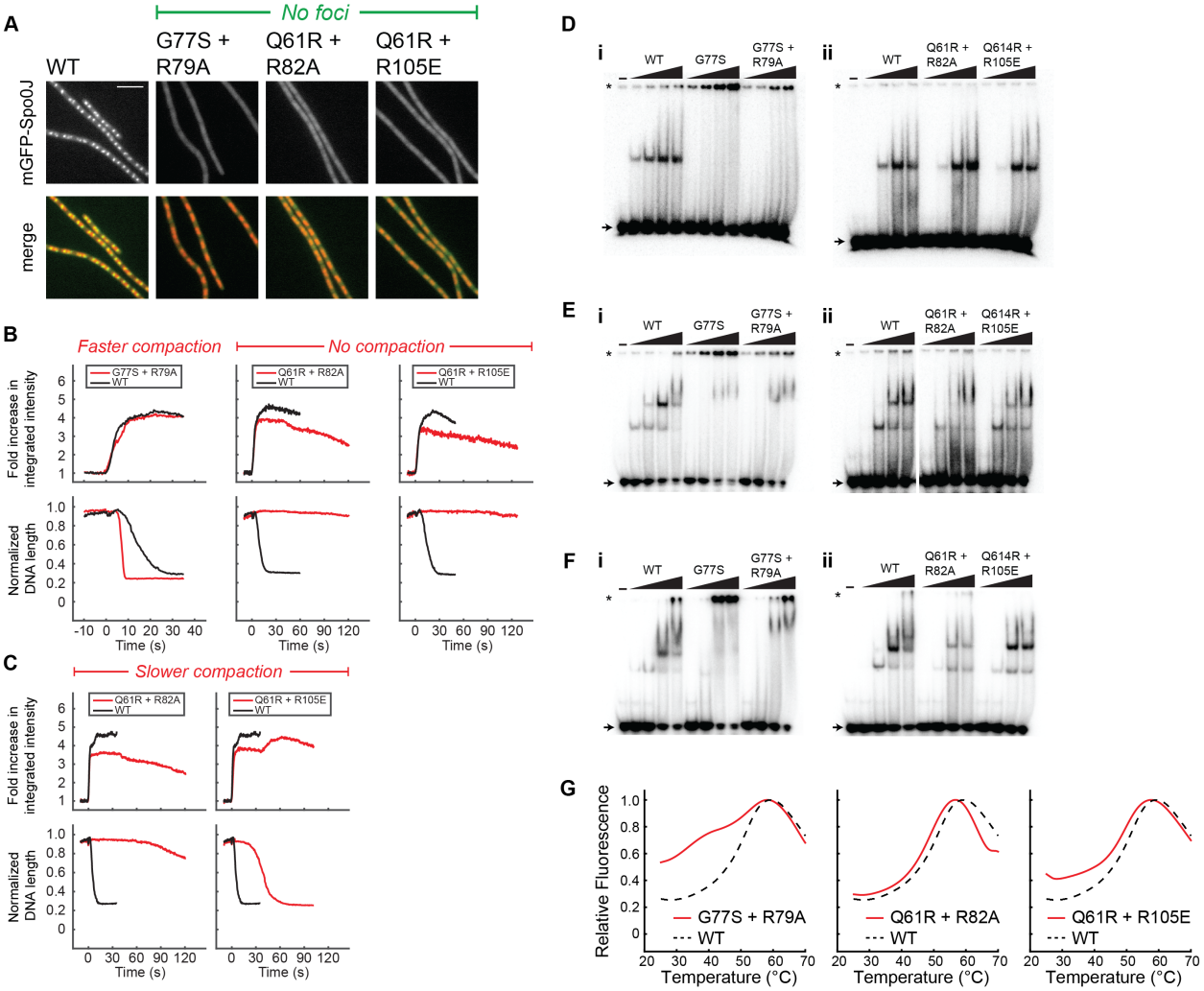

Supplementary Figure S21